Research Square

Preprints are preliminary reports that have not undergone peer review.
They should not be considered conclusive, used to inform clinical practice,
or referenced by the media as validated information.

Biases in subtropical low clouds traced to weak sensitivity to surface winds

Joaquin Esteban Blanco

joaquin_eb@hotmail.com

Stockholm University Department of Meteorology: Stockholms Universitet Meteorologiska institutionen
https://orcid.org/0000-0003-1532-2347

Rodrigo Caballero

Stockholm University Department of Meteorology: Stockholms Universitet Meteorologiska institutionen
https://orcid.org/0000-0002-5507-9209

Research Article

Keywords:

Posted Date: October 28th, 2026

DOI: https://doi.org/10.21203/rs.3.rs-10710701/v1

License: This work is licensed under a Creative Commons Attribution 4.0 International License.
Read Full License

Biases in subtropical low clouds traced to weak sensitivity to surface winds

Joaquín E. Blanco and Rodrigo Caballero

Department of Meteorology and Bolin Centre for Climate Research, Stockholm University, Stockholm, Sweden

Corresponding author address: rodrigo.caballero@misu.su.se

ABSTRACT

Models are known to systematically misrepresent cloud properties over many regions of the globe, with substantial impacts on the energy balance of the climate system. We investigate the causes of model biases in cloud albedo over tropical and subtropical stratocumulus regions using a cloud-controlling factor (CCF) method at daily timescale. We assess the performance of a 15-model CMIP6 ensemble by comparing with cloud albedo computed from CERES satellite retrievals of upwelling and downwelling shortwave radiation at the surface and top of the atmosphere and CCFs obtained from the ERA5 reanalysis. We find large negative biases in three of the major stratocumulus decks over oceans (the Californian, Peruvian and Namibian regions). However, in other areas cloud albedo errors are very small (Australian and Canarian regions). The CCF analysis shows that in all five regions observed cloud albedo robustly increases with increasing surface winds speed, in agreement with theoretical as well as Large Eddy Simulation studies. By contrast, CMIP6 simulated clouds show either small or negative sensitivity to strengthening winds. We also find that the two regions with reduced cloud albedo biases arise as error compensations of different types: excessive cloud albedo associated with ascending motion regimes (Australian), and excessive cloud albedo under weak winds (Canarian).

1. Introduction

The tropical and subtropical eastern oceans are characterized by semipermanent stratocumulus (Sc) decks, with an annual-mean coverage exceeding 40% and locally as high as 60% (Wood 2012). These low, boundary layer clouds prevail primarily within the eastern

margins of the oceanic subtropical highs, particularly over eastern boundary currents off continental regions. They are strongly coupled to both small- and large-scale processes occurring within and/or in the vicinity of the boundary layer, including surface fluxes of heat and moisture, subsidence, radiative cooling, turbulence and entrainment (Stevens 2005, Wood 2012).

Because of their strong shortwave cloud radiative effects and importance to the global energy budget, Sc clouds are among the most studied cloud types (Hartmann et al. 1992; Stevens 2005). Besides their mean cooling effect, subtropical marine clouds affect the variability of planetary-scale, low-frequency atmospheric and oceanic modes, such as El Niño–Southern Oscillation (Rädel et al., 2016; Middlemas et al., 2019), Pacific decadal variability (Bellomo et al., 2014, Hsiao et al., 2022), the Atlantic Multidecadal Oscillation (Bellomo et al., 2015, Brown et al., 2016), and even remote influences onto the Southern Ocean (Kim et al., 2022). The importance of tropical Sc and associated feedbacks has been tested in paleoclimate studies: the breakup of low-cloud decks may have contributed importantly to greenhouse climates and abrupt climate transitions in past geological eras, such as the Eocene (Schneider et al. 2019, Salazar et al. 2025). The parameterization of marine low clouds is thus critical for general circulation models (GCMs, Ceppi et al. 2017; Kawai and Shige 2020; Voigt et al. 2021).

A key issue in climate science is the understanding of how subtropical low clouds affect and are affected by current global warming, prompting studies on observed trends as well as climate projections including future cloud characteristics, emerging global patterns and circulation changes (e.g., Medeiros et al. 2008; Caldwell and Bretherton 2009; Seethala et al. 2015, Voigt and Shaw 2015, Burgman et al. 2017, Nuijens and Siebesma 2019, Bock and Lauer 2024, Breul et al. 2025). In particular, Ceppi et al. (2024) and Aerenson and Marchand (2025) have applied observational constrains to low-cloud radiative feedback and found that models underestimate the low-cloud response to warming because they systematically underestimate present-day tropical marine low-clouds. These two studies also found that the strength of the simulated cloud feedbacks have statistically significant relationships with simulations of present-day clouds. Hence, to reduce uncertainty in climate projections, it is crucial to understand and mitigate the subtropical stratocumulus biases in current models.

GCMs still struggle to adequately capture the physical processes associated with subtropical low-level marine clouds, despite decades of effort to do so (Ma et al. 1996; Duynkerke and Teixeira 2001; Siebesma et al. 2004; Bony and Dufresne 2005; Mochizuki et al. 2007; Wang et al. 2011; Boucher et al. 2013; Mechoso et al. 2014; Dal Gesso et al. 2015; Bender et al. 2016, 2019). Many studies have documented the negative biases in low-level cloudiness or their albedo in successive stages of the Coupled Model Intercomparison Project (CMIP, Meehl et al. 2000; Stevens 2024). Low-cloud errors in CMIP3 (Caldwell et al. 2013; De Szoeke et al. 2012; Lauer and Hamilton 2013) have persisted through CMIP5 (Klein et al. 2013; Su et al. 2013; Lin et al. 2014; Koshiro et al. 2018) and CMIP6 (Jian et al. 2021; Li et al. 2023; Cesana et al. 2023; Črnivec et al. 2023). A common problem detected in a range of atmospheric and coupled GCMs over tropical and subtropical oceans is that they tend to underestimate low-cloud cover but overestimate its optical thickness (e.g., Webb et al. 2001; Weare 2004; Zhang et al. 2005). This 'too few, too bright' low-cloud bias has been found in CMIP3 (Karlsson et al., 2008) and CMIP5 (Nam et al. 2012), whereas more recently Konsta et al. (2022) described the low-level marine clouds simulated by a series of CMIP6 models as 'too few, too bright but also too compact and too homogeneous'. These studies underscore the problem of compensating errors in models, some of which may correctly represent the climatological low-level cloud reflectivity but for the wrong reasons.

By applying a range of diagnostic techniques in cloud evaluations, the risks of drawing the wrong conclusions due to compensating errors are minimized (Williams and Bodas-Salcedo 2017). A typical first step to investigate the cause of the biases has been to identify whether these are due to errors in the large-scale state variables or to errors in the model parameterizations. Short-term hindcasts can provide such framework (e.g. Brient et al. 2019), and machine-learning techniques have also been explored (Lewis and Bellon 2025). The more common approach, however, is to use statistical regression analyses between clouds and their controlling factors over a long climatological period, which in turn can also be used to observationally constrain uncertainty in global warming projections (e.g. Klein et al. 2017; Myers et al. 2021; Ceppi et al. 2024).

Although many of these studies have found that most GCMs do not realistically simulate the observed relationships between low-level cloudiness and meteorological factors for tropical marine clouds (e.g., Bony and Dufresne 2005; Myers and Norris 2015; Koshiro et al. 2018; Konsta et al. 2022; Črnivec et al. 2023), timescales and variables of analysis, regions of study, models used and methodologies vary. For example, some of these studies

treat either only the sensitivity of cloud cover fraction to a given atmospheric variable, or separately from the cloud thickness sensitivity, without assessing the combined effect on radiation (i.e. cloud albedo or SW cloud radiative effect) for that variable. Another common treatment involves grouping by stratocumulus-dominant regimes versus trade cumulus regimes, without assessing why climatological negative cloud albedo biases are found for some Sc regions but not for others, whereas little or no systematic errors take place over the trade Cu regions. Furthermore, studies often focus on inversion strength or similar metrics of low-level stratification—the large-scale controlling factor that best correlates with low clouds in the tropics—while paying less attention to other variables. Last, research mostly focuses on atmosphere-only simulations, without analysing the role of ocean coupling. Here we intend to address and integrate all of these aspects.

The objective of this study is to apply a simple cloud controlling factor (CCF) framework to evaluate characteristics of clouds and their environment from CMIP6 simulations and their comparison against observations over the 2000-2014 period, focusing on five areas characterized by frequent Sc clouds, namely: the Californian, Peruvian, Namibian, Australian and Canarian oceanic regions. In a recent study, Blanco et al. (2024, hereafter B24) found that cloud albedo regressed against SST can be used a quick diagnostic calculation to detect CMIP biases of microphysical origins over the Southern Ocean, exploiting the fact that models tend to produce excessive (less reflective) glaciated clouds in contrast to the (brighter) supercooled liquid water clouds predominant over the region. Likewise, unexplored misrepresented cloud albedo–CCFs relationships over the typical marine Sc regions might point model developers into new directions to improve the performance of GCMs in simulated tropical low clouds.

The remainder of this work is organized as follows. Section 2 describes data, study regions and methods, including choice of CCFs. Results are presented in sections 3 (cloud albedo climatology for models and observations over each region) and 4 (biases from the CCF framework) and discussed in terms of existent literature in Section 5. The last section contains a summary and conclusions of this study.

2. Data and methodology

a) Observations, reanalyses and CMIP6 data

As in B24, cloud albedo is computed using shortwave (SW) radiances from Clouds and Earth's Radiant Energy Systems (CERES) Energy Balanced and Filled (EBAF) level 3 (gridded) SYN1deg daily data product Edition 4.1 (Loeb et al. 2018) for the period 2000–2014. Large-scale variables affecting observed cloudiness are derived from the ERA5 reanalysis (Hersbach et al. 2020). These CCFs are averaged to daily means and spatially regridded using linear interpolation to match the grid of the CERES data.

We use coupled ("Historical", hereinafter HIST) and atmosphere-only (AMIP, prescribed SSTs) simulation output from 15 models of CMIP6 (Eyring et al. 2016) for the same 15-year period. Only models with all daily SW radiances and CCFs for both experiments were selected. Only one realization from each model is considered (generally 'r1i1p1f1'), and equal weights are given to all models for the computation of ensemble properties. The list of models is shown in Figs. 7-9 and additional figures in the supplementary material.

b) Study regions

Although subtropical low cloud regions can be determined from satellite climatologies (Wood 2012; Cesana et al. 2019) and from specific thresholds on certain CCFs (Scott et al. 2020; Myers et al. 2021), a disadvantage of such approaches is that the statistical analysis is applied over large swaths of Earth over which the large-scale variables themselves may substantially change, even if splitting all tropical low-cloud regions into stratocumulus- and trade cumulus- dominated areas. Furthermore, not all Sc regions experience the same magnitude of model cloud biases (as will be shown), and in turn, similar annual-mean biases at different ocean basins may be due to different physical causes (as was also found).

We opt instead to adopt the five classic stratocumulus regions in narrower delimited areas (10°x10° boxes) defined as follows: Peruvian (Pe; 10°–20°S, 80°–90°W), Namibian (Na; 10°–20°S, 0°–10°E), Californian (Cf; 20°–30°N, 120°), Australian (As; 25°–35°S, 95°–105°E) and Canarian (Ca; 15°–25°N, 25°–35°W). This traditional approach that optimizes the study of Sc clouds in terms of local/regional controlling factors was introduced by Klein and Hartmann (1993) and subsequently used, among others, by Wood and Bretherton (2006), Qu et al. (2014), Muhlbauer et al. (2014), Bender et al. (2016, 2019), Jian et al. (2021), Cutler et al. (2022), Ekman et al. (2023), Zhang and Feingold (2023) and Fons et al (2024).

c) Cloud albedo

Seven variables are taken from CERES and CMIP6 models to compute cloud reflectivity: these are the combination of surface (SFC)- and top of the atmosphere (TOA)-, upwelling- and downwelling- SW fluxes, i.e.: $SW_{\uparrow}^{SFC}$, $SW_{\downarrow}^{SFC}$, $SW_{\uparrow}^{TOA}$ for all-sky and clear-sky conditions, and $SW_{\downarrow}^{TOA}$. Cloud albedo is separated from all other contributions to total reflectivity (atmospheric gases, aerosols and surface) and defined as $C = A_{all-sky}^{atm} - A_{clear-sky}^{atm}$, where A^{atm} is the atmospheric contribution to planetary albedo computed from the aforementioned SW fluxes (a full derivation can be found in Donhoe and Battisti 2011 and Stephens et al. 2015).

We note that cloud albedo can also be parameterized using cloud optical thickness and cloud cover fraction (Datseris and Stevens 2021, Blanco et al. 2023), but due to the limited availability of daily cloud properties across archived CMIP6 data, we use SW radiances instead. The two definitions can be treated as equivalent (Datseris and Stevens 2021), and both are directly applicable to gridded data (i.e., cloud albedo averages over each grid box).

d) Cloud controlling factors

Numerous studies have examined the links between global oceanic cloudiness and large-scale meteorological parameters on different time scales (e.g. Li et al. 2014, Scott et al. 2020). Focusing on subtropical marine low-level cloudiness Klein and Hartmann (1993) and Wood and Bretherton (2006) found that the inversion strength is the dominant factor that explains their geographical distribution and seasonal cycle, whereas Cutler et al (2022) found that the correlation between this parameter and cloud cover is higher for Sc clouds than for low cloud scenes in general (Sc, shallow Cu and stratus). However, these clouds are also dependent on several other factors such as momentum, energy and moisture fluxes at surface (Myers et al. 2023), subsidence strength (Myers and Norris 2013; van der Dussen et al. 2014, 2016), and entrainment at the cloud top (Mellado 2017; Koshiro et al. 2022). In addition, numerical simulations allow for the assessment of the relative contributions of these atmospheric controlling factors on the growing, maintenance or thinning/breaking up of Sc decks (Bretherton et al. 2013; Noda et al. 2014; De Roode et al. 2014).

As many studies have already assessed the role of stratification on Sc clouds in CMIP simulations (e.g. Konsta et al. (2022) and Črnivec et al. (2023) for CMIP6), we focus instead on three less-studied CCFs, namely: 500 mb pressure velocity ω_{500}; 10m windspeed $V_{\mathrm{sfc}} = (u_{10\mathrm{m}}^2 + v_{10\mathrm{m}}^2)^{1/2}$, hereafter "surface wind"; and sea surface temperature (SST).

e) CCF framework

The main method we use is the same as in B24: the response of cloud albedo to a given CCF along its full variability range is analysed by bin-averaging, i.e., binning the values at each day and grid point by the value of a CCF at the same time and location, and then averaging within each bin. This results in a cloud albedo response function $C(x) = C_x$ where x is a given CCF. This simple regression technique is advantageous as it keeps the full nonlinearity of cloud albedo as a function of the large-scale variable, in contrast to other CCF methods using linear regressions. The climatological cloud albedo $\bar{C}$ is obtained by weighting C_x by the frequency of occurrence over each bin, and then integrated over all bins, yielding the expression:

$$\bar{C} = \int C_x \, P_x \, dx \qquad (1a)$$

where $P(x) = P_x$ is the climatological probability of x, computed as normalized histograms over the same bins used to calculate C_x. Note that $\bar{C}$ does not depend on the choice of CCFs, i.e.: all integrations (computed over the entire variability range of the CCFs) converge to the same the climatological cloud albedo value. The same method can be extended to n dimensions. If n=2, two CCFs can be simultaneously used to predict $\bar{C}$, i.e.:

$$\bar{C} = \int C_{x_1 x_2} \, P_{x_1 x_2} \, dx_1 \, dx_2 \qquad (1b)$$

Eq (1) is applied separately to each Sc region for CERES & ERA5 as well as for each of the CMIP6 members. In all cases the CCF method is applied on its native spatial resolution (so the total number of elements while bin-averaging is greater for higher resolution models), although the resulting averages are on a uniform grid as we use 40 equispaced bins spanning the range of each CCF, ensuring smooth variations in the C_x functions. The bin-averaging method uses area weighting (cosine of latitude) for the calculation of C_x and P_x.

Following eq (2a), the cloud albedo bias for a given CMIP6 model is calculated as

$$\Delta\bar{C} = \bar{C}^M - \bar{C}^{OBS} = \int [C_x^M \, P_x^M - C_x^{OBS} \, P_x^{OBS}] \, dx \qquad (2a)$$

where the *M* superscript stands for a CMIP model and the OBS represents satellite and/or reanalysis data. It can be further re-arranged as:

$$\Delta\bar{C} = \frac{1}{2}\int (C_x^M + C_x^{OBS})(P_x^M - P_x^{OBS}) \, dx + \frac{1}{2}\int (C_x^M - C_x^{OBS})(P_x^M + P_x^{OBS}) dx$$

$$= \Delta\bar{C}_x^A + \Delta\bar{C}_x^B \quad (2b)$$

The term $\Delta\bar{C}_x^A$ represents the part of the bias attributable to the errors in the large-scale state variable *x,* whereas the term $\Delta\bar{C}_x^B$ term is associated to errors in cloud parameterizations and/or in other large-scale controlling factors that project onto the cloud response function to *x*. If $C_x^M = C_x^{OBS}$ while $P_x^M \neq P_x^{OBS}$, then $\Delta\bar{C} = \Delta\bar{C}_A$ and the entire bias is fully explained by differences in the histograms of x. In the opposite limit, $C_x^M \neq C_x^{OBS}$ while $P_x^M = P_x^{OBS}$, in which case none of the cloud albedo bias can be attributed to *x*. For example, in the particular case that $C_x^{OBS}$and C_x^M have very similar or identical shapes such that the difference between them yields approximately a constant value, it follows that the $\bar{C}$ bias (either positive or negative) cannot be explained by x, since for any value of x, the model under/over-estimates *C* by the same amount so other factors must be the cause of the errors, and at best it may be said that the $\bar{C}$ bias occurs over a preferred range of x (determined by P_x^{OBS} and P_x^M).

Finally, as bias $\bar{C}$ change across regions and models, it is useful to normalize by expressing the relative contribution of each term to the total bias, as follows:

$$1 = A_x + B_x$$

$$A_x = \Delta\bar{C}_x^A/\Delta\bar{C}$$

$$B_x = \Delta\bar{C}_x^B/\Delta\bar{C} \quad (2c)$$

We further note that while in principle the method (eqns. 1–2) can be applied to any variable, additional criteria should be considered to assess skill in bias prediction. For example, if little or no sensitivity is found for C_x^{OBS} (i.e.: $\frac{dC_x^{OBS}}{dx} \sim 0$), then x is either a poor CCF or the control it exerts on Sc clouds is neutralized by other factors. Also, the situation where $\frac{dC_x^M}{dx}$ and $\frac{dC_x^{OBS}}{dx}$ have opposite sign (e.g. simulated clouds increasing with increasing x but observed clouds decreasing) will likely imply notorious problems in cloud parameterization related to x compared to the case in which $\frac{dC_x^M}{dx}$ and $\frac{dC_x^{OBS}}{dx}$ have the same sign. These concepts will be referred to when discussing results.

3. Model biases in cloud albedo over the subtropics

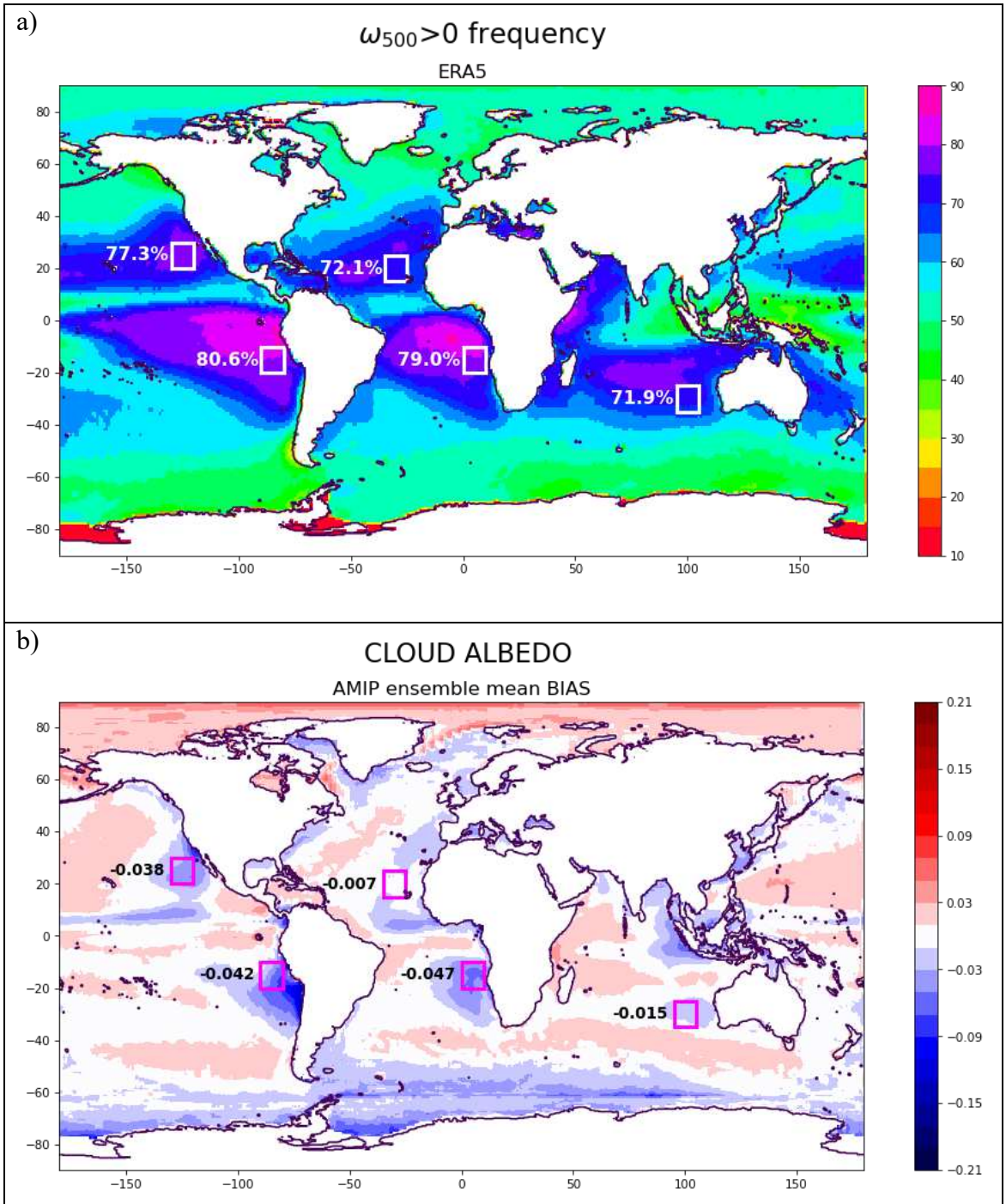

Figure 1: Annual-mean frequency (%) of positive midlevel pressure velocity from reanalysis (a), and ensemble mean cloud albedo biases for AMIP simulations (b). Displayed values are averages over the five Sc regions.

Figure 1a shows the climatological frequency of 500mb subsidence from ERA5. Tropical and subtropical areas with high subsidence frequency correspond well with the typical low-cloud regions identified in previous work (Wood, 2012), although further refinement such as the separation between mean stratocumulus and trade cumulus regions can

247 be obtained by considering the covariation of pressure velocity and inversion strength (Scott
248 et al 2020, Myers et al 2021). Subsidence frequency in the five study boxes ranges from 71–
249 81%, with the largest value off the coasts of Peru and the smallest west of the Canaries and
250 Australia.

251 The regional distribution of ensemble-mean $\bar{C}$ bias (CERES–AMIP) is depicted in
252 Fig. 1b (results for individual members can be found in Fig. S1). Over the tropical and
253 subtropical Sc regions, negative biases are found in proximity to the coasts, but the
254 magnitudes vary. In particular, the Peruvian zone exhibits the largest bias among the five
255 regions, although the peak does not exactly fall within the corresponding box as defined in
256 Section 2, but shifted Southeast, encompassing coastal areas of Peru and Chile. Ensemble
257 mean negative biases are smaller for the Australian and Canarian regions. Nearly identical
258 results are shown by Črnivec (2023; their Fig. 4) albeit for a different set of AMIP models
259 and period of analysis: positive SW cloud radiative effect biases (proportional to negative $\bar{C}$
260 biases) were found largest for Pe, Na and Cf regions, with either small or negligible biases in
261 the remaining two regions. In addition, we find a very similar bias pattern when the same 15
262 models are evaluated in the coupled configuration (HIST ensemble, Fig. S2b).

263 The subsidence frequency from the AMIP ensemble (Fig. S2a) shows larger values than
264 in the ERA5 reanalysis over all the Sc boxes, ranging from 73–85%. This bias in subsidence
265 climatology can potentially support the negative $\bar{C}$ bias of Fig. 1b, given that enhanced
266 subsidence tends to reduce subtropical marine boundary layer cloudiness (Myers and Norris
267 2013). To what extent variations in subsidence strength affect observed and simulated
268 cloudiness will be analysed later.

269 We next evaluate ensemble spread in both AMIP and HIST ensembles considering
270 area-averages over the five Sc boxes (Fig. 2). The group with larger biases (Peruvian,
271 Namibian and Californian regions) is also characterized by larger spread, and by overall
272 smaller errors in the atmosphere-only configuration. Noteworthy is the Australian region,
273 with very similar AMIP and HIST distributions, and with the two ensembles' median slightly
274 positively biased compared to the CERES climatology.

275 Individual model skill is further shown in Figs. S3 and S4. For the Pe-Na-Cf group
276 (Fig. S3) only a handful of models produce the right (or almost) amount of cloud albedo at a
277 given location, and only one (HAMMOZ-MPI AMIP) at any two of these three regions.
278 Although some models simulate excessive cloud reflectivity, the great majority of

simulations produces a deficit, usually in the three areas. In turn, over the Canarian region models tend to a fairly good performance, except for all members from the NCAR family (Fig. S4). While some models generate identical annual-mean $\bar{C}$ in both atmosphere-only and coupled configuration, there is a great variety across the ensemble, and dependence on geographical location.

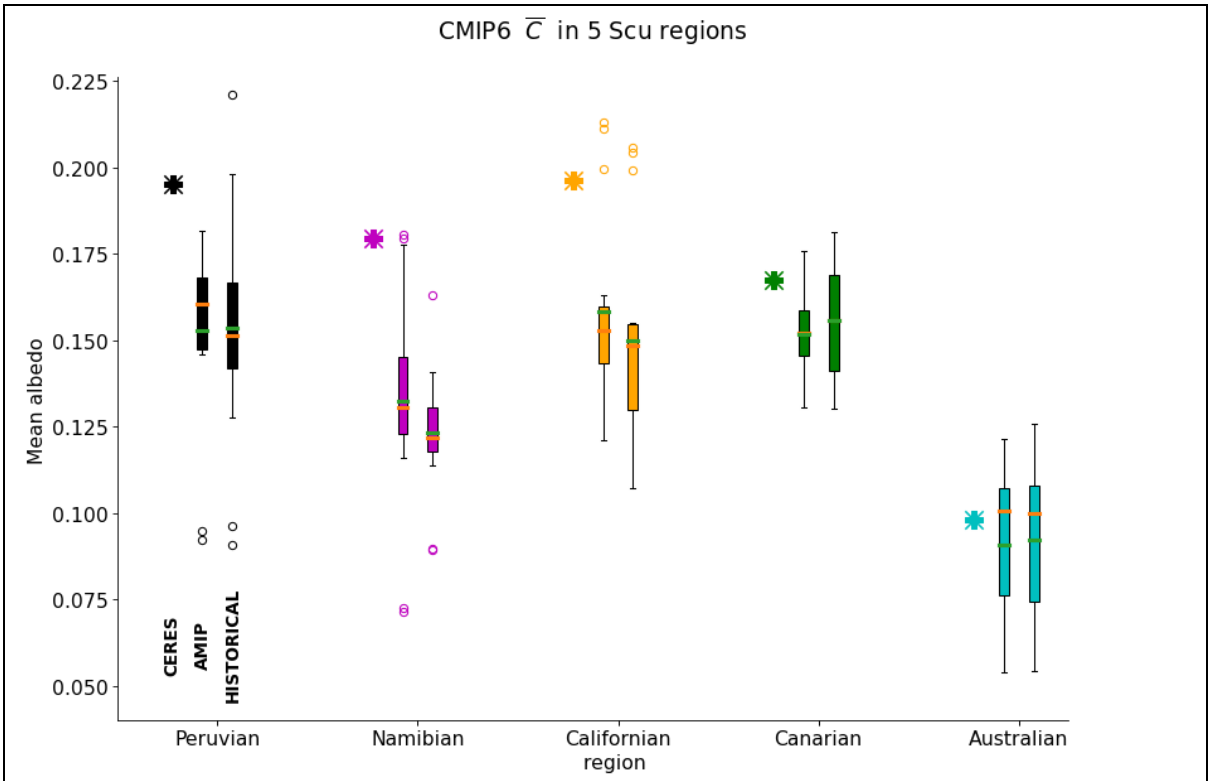

Figure 2: Annual mean cloud albedo computed as area-weighted averages for the 5 oceanic Stratocumulus regions. For each case, the heavy star denotes the CERES observation whereas the left (right) box plot shows the distribution of the 15-member AMIP (HIST) ensemble. Mean (median) is indicated by a green (orange) stripe. Box boundaries represent Interquartile Range (IQR), whiskers extend to the furthest data points within 1.5×IQR, and all values exceeding those limits are depicted by open circles.

4. CCF analysis of cloud albedo biases

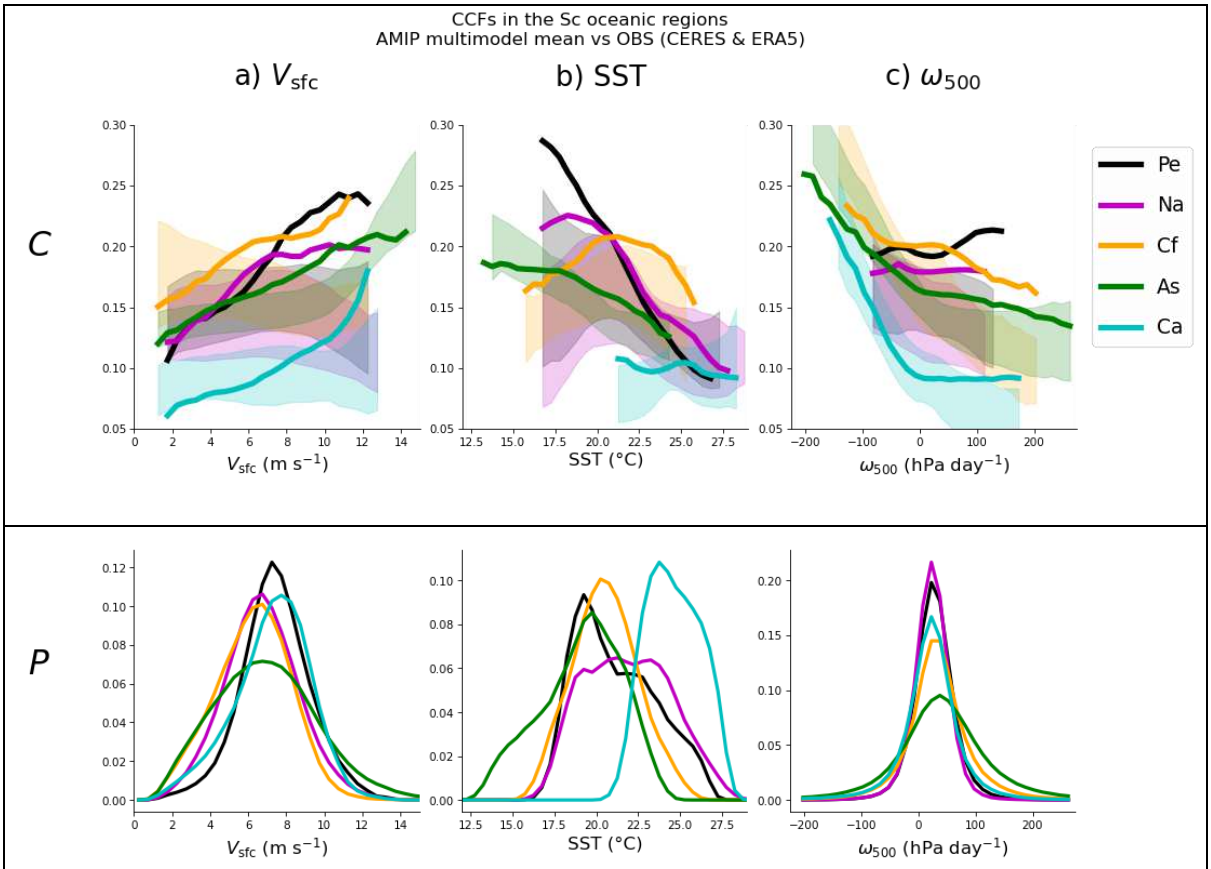

Figure 3: One-dimensional CCF analysis of observed (CERES & ERA5) cloud controlling factors for the five Stratocumulus boxes (solid lines). Top: Cloud albedo regression functions (*C*) for the three CCFs as indicated above, and bottom: probability density functions (*P*) of the CCFs. Shading in the top panel indicates the spread of the AMIP ensemble for each region, computed as the ensemble mean ±1 standard deviation.

4a) CERES & ERA5

Before analysing simulated clouds in terms of their CCFs it is important to examine the observations in some detail, given the peculiarities associated with local climatologies of each region. These characteristics are depicted in Fig. 3.

Under typical conditions in trade Cu and Sc regions, surface wind affects surface turbulent fluxes and thus boundary-layer thermodynamics and cloudiness. Observational, theoretical and large-eddy simulation studies agree that increasing surface wind induces adjustments in the boundary layer favouring thicker low-level clouds with greater fractional cover and an increase in cloud-top height (Nuijens and Stevens 2012, Bretherton et al. 2013, Kazil et al. 2016, Mieslinger et al. 2019). As cloud albedo is a function of optical thickness

and fractional cover, we expect it to increase with increasing surface wind. Consistently, we see *C* increase with increasing winds robustly in all Sc regions (Fig 3a, see also Blanco et al 2023). Although the relationship is quasi-linear with very similar slopes in all areas, the Canarian box stands out as markedly less cloudy than the others, likely due to the influence of underlying warmer SSTs (see below). The most frequent wind speed intensity in all regions ranges between 6–8 m/s.

Overall, cloud albedo decreases with increasing SST (Fig. 3b), and the substantial P_{SST} shift to warmer temperatures over the Canarian region (most frequent SST value at around 24°C) helps explain its smaller albedo compared to the other four regions. The negative $dC_{SST}/dSST$ response agrees with previous observational and modelling evidence in the extended tropical and subtropical oceanic areas (Bony and Dufresne 2005; Rieck et al. 2012; Bretherton and Blossey 2014. Qu et al. 2015, Scott et al. 2020). It has been proposed that colder temperature reduces the efficiency of entrainment and thus diminishes the rate of cloud top evaporation, although the precise mechanism remains debated. However, Fig 3b shows that for sufficiently cold oceans, the relationship reverses and lowers SST favours lower cloud albedo (Californian and to some extent Namibian regions). The C_{SST} curve for the Canarian region is even more peculiar, with reduced sensitivity to temperature changes and a pattern of multiple reversals (increase to decrease and vice versa), although this occurs towards the warm end of the temperature range.

In general, stronger ascents tend to enhance cloudiness, whereas subsidence favours its inhibition and suppression (Fig. 3c), in line with expectations from cloud dynamics in the tropics and extratropics. A notable exception, however, occurs over the Peruvian box, with cloudiness increasing with increasing subsidence for ω_{500} >30hPa/day, and a relative maximum at ω_{500} = -20hPa/day. The increase of cloudiness with increasing subsidence strength may be explained by a countering effect exerted by lower tropospheric stability: if on the one hand enhanced subsidence favours drying of the boundary layer and overall cloud thinning, on the other hand a stronger cloud-top inversion exerts a moisture-trapping role by reducing entrainment of drier air from the free troposphere (the interplay between both CCFs is addressed in Myers and Norris 2013).

4b) AMIP simulations

The top panel of Fig. 3 also shows the spread in the AMIP simulations of the *C* regression functions for each CCF. Despite geographical differences, models tend to underestimate cloudiness under subsidence conditions whereas they more accurately capture the increase of albedo with increasing ascent strength, albeit with overestimations in some regions (Fig. 3c). The overall pattern for SST (panel b) is a considerable negative bias, although the ensemble seems skilful in simulating the rate of change in cloudiness per change of SST. In terms of surface wind (Fig. 3a), models typically predict an incorrect pattern: cloud albedo is either insensitive to V_{sfc}, or it decreases with wind intensity, contradicting the CERES & ERA5 empirical findings. The Australian region is an exception, where cloudiness increases sharply with increasing wind above 10 m/s.

We next provide a more detailed analysis of CMIP6 biases taking also into account the simulated frequency of occurrence of each CCF (*P* distributions), and we analyse regions separately. Over the Peruvian region (Fig. 4), the most frequent wind speed for the AMIP ensemble is ~6.5m/s, with a less pronounced peak compared to observations, and a slight shift of the distribution towards weaker intensities. The latter compounds with the large differences between $C^{M}_{V_{sfc}}$ and $C^{OBS}_{V_{sfc}}$ at high wind speeds to give large combined effect (*CP*). The annual-mean negative bias for AMIP simulations is thus linked to the increasingly poor cloud representation by models under increasing surface winds. By similar arguments, model errors are correlated with reduced cloud albedo over colder SSTs. There is a difference, though, with the one-dimensional CCF analysis applied to ω_{500}: strong cloud albedo biases are present for all values of vertical velocity, and with little *C* sensitivity over the ω_{500} range where the bulk of the data is concentrated. But models underrepresent cloud reflectivity even for extreme positive or negative ω_{500}, implying that factors other than ω_{500} must be responsible for the negative $\bar{C}$ biases. In contrast, for certain ranges of SST and V_{sfc}, models simulate the right cloud albedo amount, beyond which model biases become positive. By combining results, negative $\bar{C}$ biases over the Peruvian region maximize with the co-occurrence of strong winds and a colder oceanic surface. A similar pattern is found for the Namibian area (Fig. S5), although with a substantial error reduction under ascending regimes.

Unlike the tropical Pe and Na regions, which are located equatorward of 20°, the Californian box is located poleward of that latitude and more exposed to extratropical influence especially during wintertime. Here, moderate ω_{500}<0 regimes occurring more frequently (Fig. 3c), although not as much as in the other two subtropical regions, Ca and As.

363 However, over the latter three subtropical regions, models are skilful in reproducing a strong
364 $C_{\omega_{500}}$ sensitivity in line with observations (Figs. 5, S6 and S7), and even positive albedo
365 biases.

366 The CCF analysis over the Californian box (Fig. S6) indicates that there is a broad SST
367 variability for this region, and models accurately depict the rate of change of C_{SST} but with a
368 deficit in albedo for any SST value. This suggest that cloud controlling factors other than SST
369 should explain the negative $\bar{C}$ biases. In turn, these climatological biases are associated with
370 reduced cloudiness under moderate-to-strong winds, and under weak subsidence.

371 Regarding the Canarian region (the one with the smallest $\bar{C}$ bias in multimodel mean), a
372 different pattern is found. The $C_{V_{sfc}}^{M}$ curve shows almost no sensitivity to wind, notably
373 differing from the corresponding CERES-ERA5 regression function (Fig. 5). But unlike other
374 regions, the nearly constant value of C~ 0.8–0.9 implies both over- and under-estimations
375 compared to the $C_{V_{sfc}}^{OBS}$. Thus, the negative bias associated with strong winds are largely
376 compensated by the positive bias under near-calm conditions. In turn, models have an overall
377 good cloud representation under ascending motion and weak subsidence, but negative biases
378 grow with increasing subsidence strength.

379

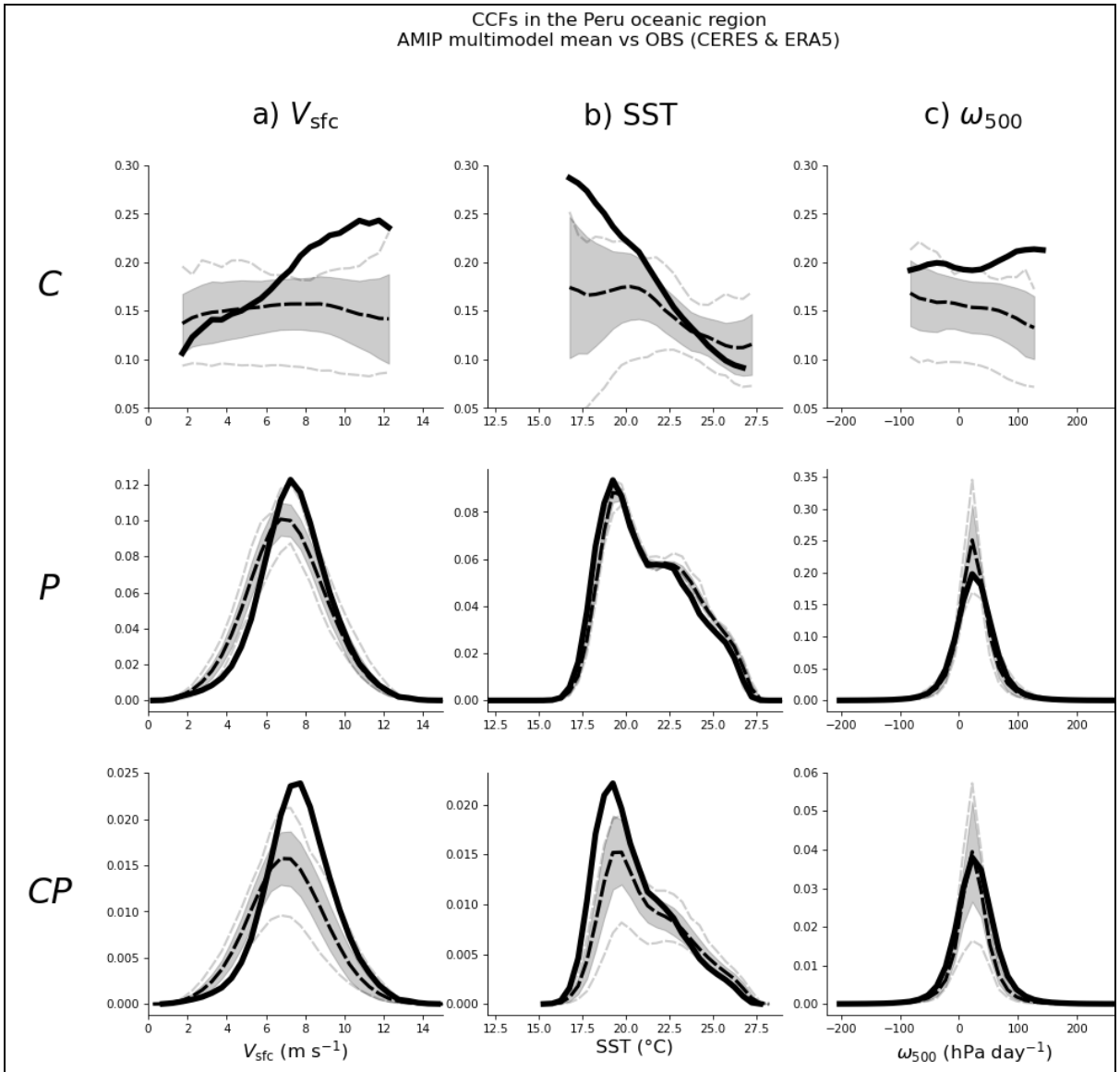

Figure 4: CCF analysis for the Peruvian region. Cloud albedo regression functions (*C*) for the three CCFs as indicated at the top (first row); probability density functions (*P*) of the CCFs (middle row); product of *C* and *P* (bottom row). AMIP ensemble means (dashed lines), inter-model spread (one standard deviation, light shading), and extremes (dashed, light) are shown, while observations (CERES/ERA5) are in solid, heavy lines.

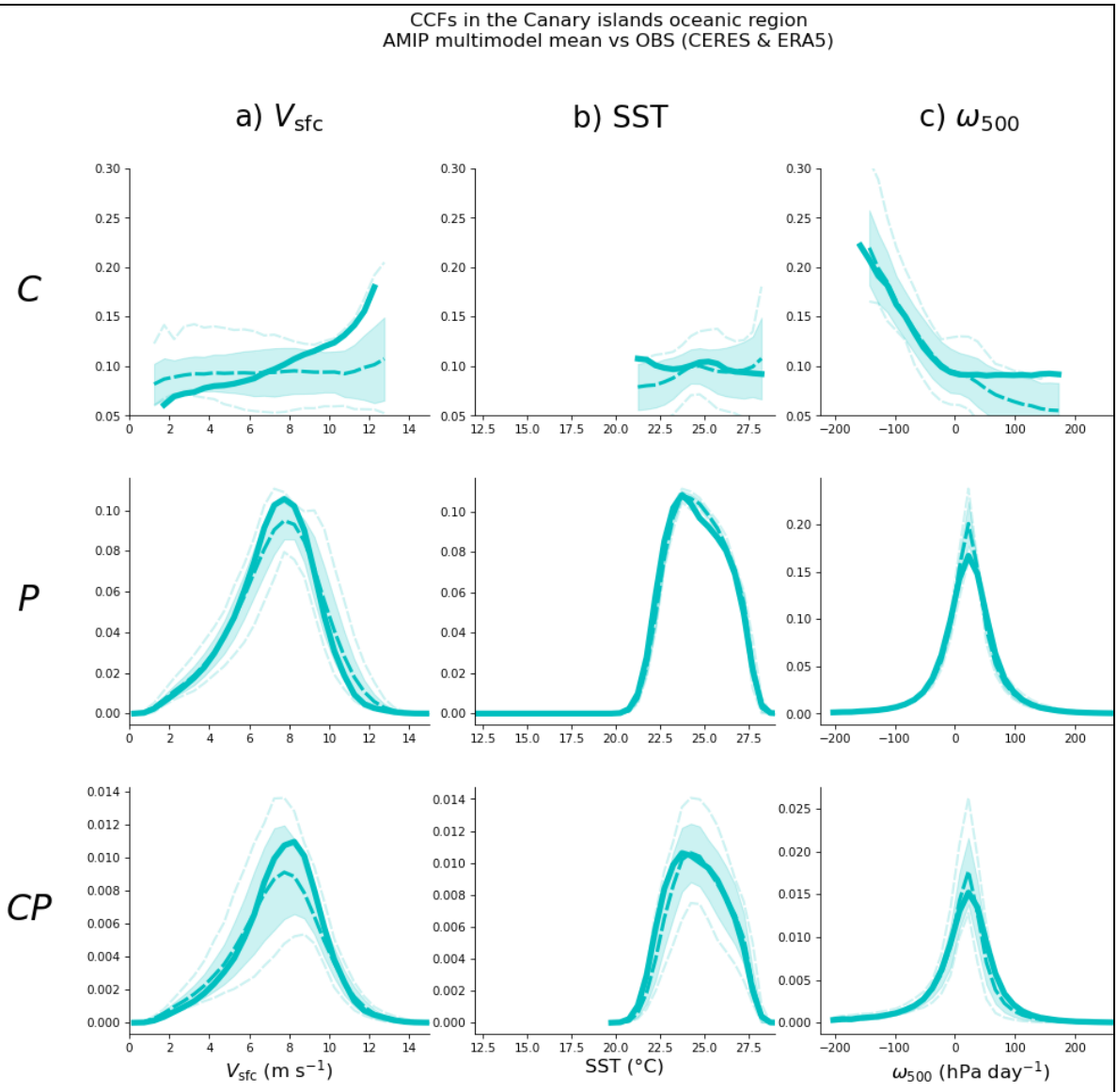

Figure 5: As in Fig. 4 for the Canary Islands region.

4c) Ocean coupling effect

Despite the small ensemble-mean differences between AMIP and HIST experiments (Figs. 2, S3 and S4), we next repeat the CCF analysis on the HIST ensemble for additional insight. Focusing on the Peruvian region, Fig. S8 shows the equivalent of Fig. 4 for the coupled configuration, with the key difference among all panels being the warm SST bias of the Southeast Pacific, a systematic phenomenon present in CMIP5 and CMIP6 (Hourdin et al 2015, Zhang et al. 2023) and largely attributed to the SW surplus at the ocean surface produced by deficits in low-level cloudiness (although other effects such as insufficient oceanic cooling via evaporation, weak coastal upwelling and low ocean model resolution

may also contributing). Signs of a low-cloud –SST feedback mechanism in coupled simulations are nevertheless inconsistent with the AMIP results, as simulations forced with observed (colder) SST do not simulate the observed amount of cloudiness, and not even necessarily larger than for the HIST simulations.

Poor model physics can be interpreted in a one-dimensional CCF analysis by the much smaller sensitivity of simulated clouds to SST forcing (C_{SST}^{M}) compared to observations. Therefore, the impact of changes in the shape of the *P* distribution when multiplied by *C* is largely reduced. Particularly over the Peruvian region (Fig. S8), it is notorious that the warm SST bias translates into a slightly larger cloud albedo climatology for the HIST ensemble mean than for the AMIP average (Fig. 2). The Namibian region is also characterized by a substantial warm SST bias (Fig. S9), but in this case the oceanic coupling is linked to a multimodel mean net reduction in cloud albedo (Fig. 2). If the median of the ensemble is considered instead, there is a net albedo decrease (bias increase) from AMIP to HIST in both Pe and Na regions, in agreement with expectations.

On the other hand, the two regions with smallest climatological cloud albedo biases (Canarian and Australian) show little changes in the normalized SST histogram compared to the AMIP ensemble (Fig. S9 vs Figs. 5 and S7), consistent in a low-cloud –SST feedback sense. For the remainder of this study, we will focus our analysis mainly on the AMIP ensemble.

4d) Individual model performance

Although Figs. 4 and 5 show multimodel properties beyond the mean, it can be illustrative to oversee the behaviour of individual members, and we next focus on V_{sfc}. The poorest-performing members over the Pe and Na regions are the two from the CNRS group, which stand out from the ensemble: they produce extremely low cloud albedo which further decreases with strengthening wind, amplifying biases (Fig. 6a,b). Over the Californian region both low- and high-resolution version of the MPI model produce too high *C* values for weak winds, whereas for most of the wind range the largest negative biases in Cf are again for the CNRS models (panel c). Over the Canarian box CanESM5 simulates excessive cloud albedo whereas members of the NCAR family have the largest deficit.

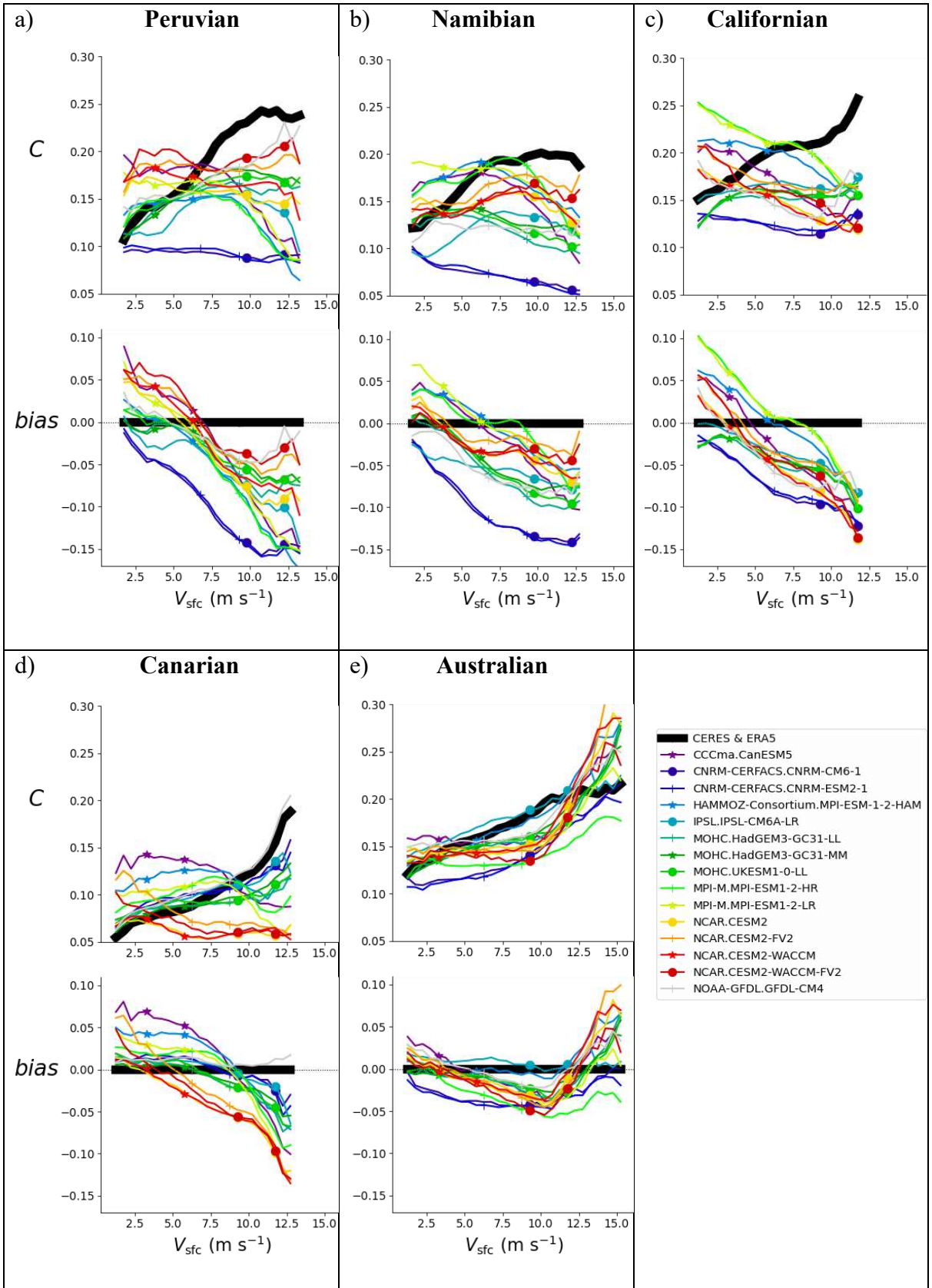

Figure 6: $C_{V_{sfc}}$ regression functions for each AMIP simulation at the respective Sc regions (panels a-e), and their corresponding biases relative to CERES & ERA5.

425

To better appreciate which models are skilful in representing $C_{V_{sfc}}^{OBS}$, it is useful to group curves by regions for each member of the ensemble (Figs. S10 and S11). It can be seen for example, that the two CNRS models, IPSL and GFDL follow the observed curve for the Canarian region rather accurately, and the same can be said for the HAMMOZ-MPI and IPSL models over the Australian region.

We apply our bias attribution method (eq 2) to determine for each model and region, which percentage of the $\bar{C}$ bias can be attributed to errors in a given cloud controlling factor or to errors in cloud parameterizations (and/or other CCFs). Skill score values (B) close to unity imply relatively large errors in C_x compared to errors in P_x. Results for surface wind summarize the model difficulties to predict $C_{V_{sfc}}^{OBS}$ in proper manner, with most scores exceeding 80% (Fig. S12). A few exceptions are found, such as HAMMOZ-MPI for the Cf region. We note that these scores do not necessarily reflect the skill in $C_{V_{sfc}}$ that can be qualitatively inferred from Figs. 6, S10 and S11, as they also incorporate information from the observed and predicted wind frequencies. A similar picture is obtained if the B skill score is applied to ω_{500} (Fig. S13). These combined results suggest that climatological biases could be linked to deficiencies in cloud parameterizations.

By design, prescribed SST in the AMIP experiment imply $P_{SST}^{M} = P_{SST}^{OBS}$ so that the bias skill score B equals unity. This result can be used to quantify the relative impact of the warm SST bias in the $\bar{C}$ climatologies of the coupled simulations. Fig. S14 shows a wide range of variation of these scores across models and regions. As expected, for the Namibian and Peruvian regions, the disproportionally warm ocean surface account for 40% of the biases, in the ensemble mean, a value that reduces to ~15% over the Canarian region (note that even with no warm SST bias as determined by the mode of the distributions, errors in P_{SST} shape are pronounced; Fig S9b).

Figure 7: Cloud albedo sensitivity to subsidence-only (+ symbols) conditions for AMIP simulations, in the Canarian and Australian regions. The climatological albedo for all conditions is shown as in Fig. S4.

451

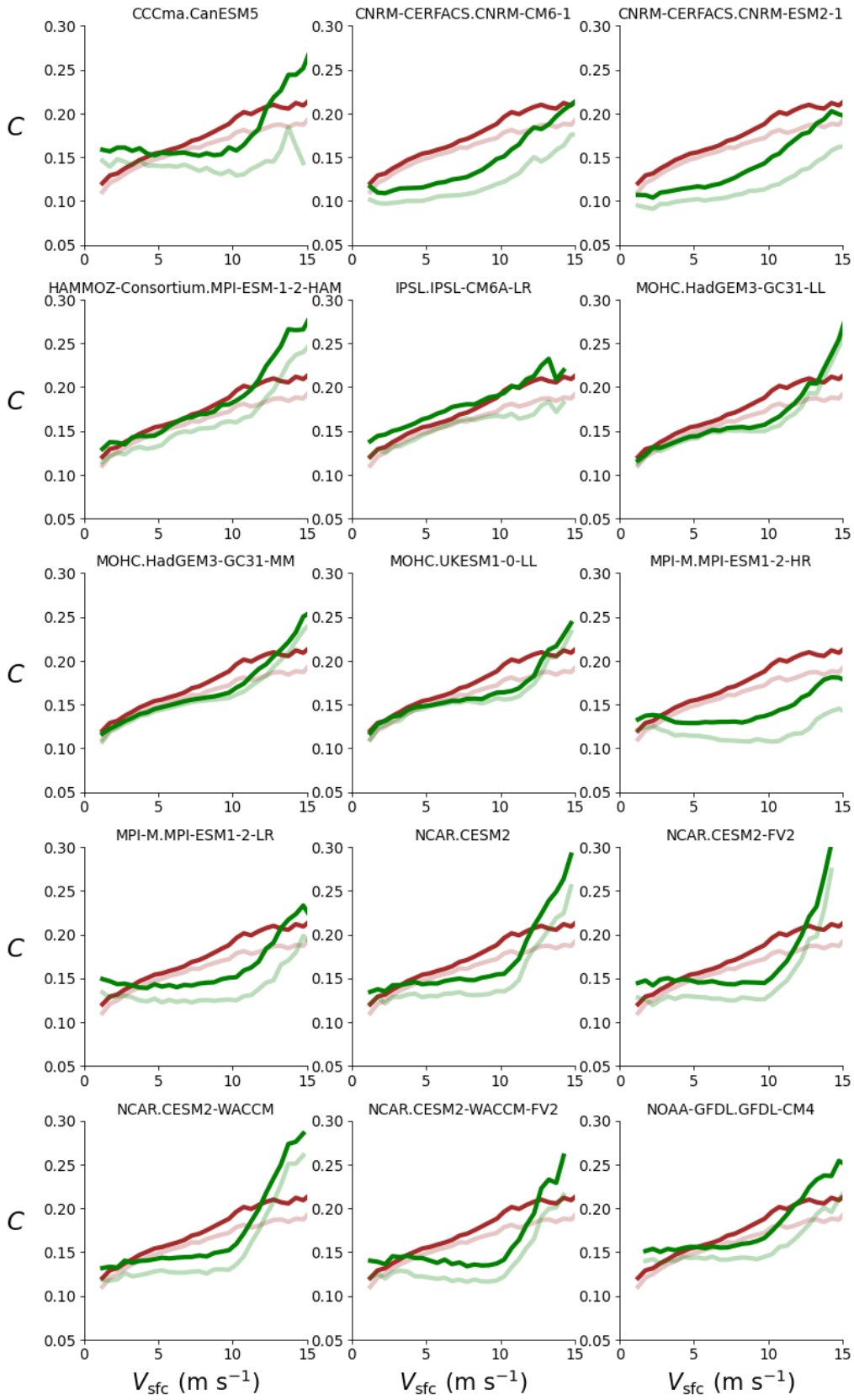

Figure 8: $C(V_{sfc})$ sensitivity to subsidence-only conditions in AMIP simulations, for the Australian region. Full (light) colour shows all (subsidence-only) conditions. Brown (green) colour is used for CERES & ERA5 (AMIP).

4e) Sensitivity to subsidence-only conditions

As seen from Figs. 3a and 6, perhaps the most intriguing oceanic region is the one west of Australia, not only for the much smaller spread compared to the other four areas when comparing $C^{M}_{V_{sfc}}$, but also because the totality of models captures the albedo increase with strengthening winds for V_{sfc} >10 m/s, although not in the same fashion as in $C^{OBS}_{V_{sfc}}$. To assess the potential role of wintertime cyclonic activity (combination of enhanced winds and ascending motion in the generation of clouds), we applied a subsidence-only filter to our data and recomputed the $\bar{C}$ climatology as well as the $C^{M}_{V_{sfc}}$ curves. Figure 7 shows that although $\bar{C}$ decreases both for AMIP and OBS in association with the removal of the too-high albedo scenes under ascending motion (Fig. S7), the negative $\bar{C}$ bias shows little change. Second, in the albedo curves regressed against surface wind (Fig. 8), it is noteworthy that the ensemble of $C^{M}_{V_{sfc}}$ overall maintain the shape, that is, predicting a *C* increase with increasing V_{sfc}. In summary, models as a whole fail to reproduce the $\frac{dC}{dV_{sfc}} > 0$ empirical finding within cloud-topped boundary layers dominated by subsidence and stratification, in four of the five traditional stratocumulus clouds regions, although in the remaining one the rate of increase substantially deviates from observations.

5. Discussion

Although our simple CCF framework (eqs. 1–2) can straightforwardly be extended to two or three dimensions to assess the combined effect of our set of CCFs, such approach may hinder the interpretation of physical processes in both observation and models. Therefore, we next bring together the results of the application of the CCF separately for each variable, alongside relevant considerations regarding inversion strength.

The three Sc regions with largest $\bar{C}$ biases are Pe, Na and Cf. For these, models overall simulate $P_{\omega 500}$ accurately and the bulk of the distributions occurs for the range 0– 50 hPa/day, characterized by reduced $C^{OBS}_{\omega 500}$ albedo variability. There are large positive differences $C^{M}_{\omega 500} - C^{OBS}_{\omega 500}$ over the Peruvian and Namibian areas (and also within Cf for ω_{500} > -50 ω_{500} hPa/day) suggesting that other factors must play a more determinant role. The subsidence removal test over the Australian and Canarian regions (sporadic ascents do have an impact in the enhancement of annual-mean cloud albedo), further demonstrated that the net effect on $\bar{C}$ biases is negligible due to similar changes in observed and simulated

482 climatologies. To summarize, at best it can be said that $\bar{C}$ biases in Sc regions occur in
483 presence of subsidence conditions, which is by nature a characteristic of the Sc regimes
484 themselves.

485 Similarly, little insight can be gained from the assessment of SST effect on low-cloud
486 model representation, even if excluding HIST simulations from the analysis. Larger biases
487 occur under colder ocean surfaces in the Pe and Na regions, but for all the temperature range
488 over Cf. Local effects are such that C_{SST} is non-monotonic for this region, with albedo
489 decreasing with decreasing SSTs, but opposing the observed pattern in the other two areas.
490 Thus, these findings obscure the true physical mechanisms of SST as a Sc controlling factor,
491 let alone its potential role on the $\bar{C}$ biases.

492 While studies have historically agreed on the importance of vertical velocity and
493 inversion strength in controlling low-level cloudiness in the typical trade Cu and Sc regions
494 of the marine tropics and subtropics, it has become increasingly clear that V_{sfc} is another key
495 player (e.g. Nuijens and Stevens 2012; Kazil et al. 2016; Mieslinger et al. 2019; Scott et al.
496 2020). Regarding CMIP6 simulations of the ~2000-2014 period, the wind effect on cloud
497 cover fraction has been assessed in Konsta et al (2022) for a set of six models, and despite the
498 integration over the entirety of the tropical oceans, it also reveals reduced sensitivity
499 compared to observations (their Fig. 3d). However, the net role of V_{sfc} on radiative properties
500 of clouds (i.e.: cloud albedo C, combining cloud fraction and optical thickness effects) was
501 not explored.

502 In principle it can be said that $\bar{C}$ biases over Pe, Na and Cf regions occur in presence
503 of moderate-to-strong surface wind speeds. However, unlike SST and $\omega_{500,}$ the strong albedo
504 sensitivity to wind intensity is further characterized by quasi-linearity with similar increase
505 rate for all study regions, and for the entire variability range of V_{sfc}. Furthermore, this
506 robustness adds up to theoretical arguments, and large-eddy simulation results supporting the
507 important role played by wind on cloud generation. A relevant aspect is that despite multiple
508 complex boundary layer processes affecting cloud formation, maintenance and suppression,
509 oceanic evaporation directly (and linearly) depends on surface wind strength in bulk
510 aerodynamic formulations of surface turbulent fluxes. Another important point is that V_{sfc} (or
511 more properly, wind shear) is likely having opposing effects at different levels and/or stages
512 of Sc dynamics: if enhanced turbulent kinetic energy favours cloud thinning via entrainment
513 and evaporation at the top of the boundary layer, it must be at a smaller rate than the

514 enhanced oceanic surface evaporation, low-level moistening and subsequent condensation, in
515 order to sustain the net cloud growth seen in Fig. 3a.

516 When contrasting CMIP6 models to the empirical evidence and theoretical concepts,
517 it is immediate that they are extremely deficient in representing observed sensitivities, as they
518 simulate $\frac{dC}{dV_{sfc}} \sim 0$ or even negative. These results suggest that cloud parameterization errors
519 in Sc regions likely relate to improper $C^{M}_{V_{sfc}}$. We note that a more detailed analysis would be
520 required to understand why the Australian area is unique in terms of $C^{M}_{V_{sfc}}$ (smaller
521 intermodel spread, smaller biases, and overall albedo increase with increasing wind strength),
522 compared to the other four regions.

523 Although inversion strength was not directly analysed in this study, it is worth
524 discussing the implications of some observational as well as CMIP6 findings. One of the key
525 characteristics that distinguish typical trade Cu regimes from Sc- regimes is the stronger
526 inversion for the latter (Estimated Inversion Strength > 1 K), compared to the generally
527 weaker inversion of the former (EIS < 1 K). Trade Cu regions are adjacent and west of the Sc
528 regions and extend over large swaths of the respective oceanic basins (e.g. Fig. 3 in Scott et al
529 2020), but as our Figs. 1b and S2b show, ensemble mean CMIP6 biases are either very small
530 or negligible over trade Cu areas. This indicates that the large negative $\bar{C}$ biases occur in
531 presence of high EIS conditions, although high EIS values do not per se imply large negative
532 biases, as the Ca and As regions demonstrate.

533 Figure 1 in Črnivec et al (2023) shows that CMIP6 models systematically
534 underrepresent inversion strength in subsidence regimes of tropical oceans (all EIS
535 histograms shifted to smaller values compared to observations). As cloudiness increases with
536 increasing EIS, it yields following eqs. 1–2 that biases are partly due to poor simulation of the
537 EIS climatology. Equally important, the right panel of their Fig.1 also shows that although
538 models have a similar rate of change of cloudiness per change of EIS, there is a negative
539 offset between the most models and observations, implying that other factors must be also
540 partly responsible for the negative biases, for any given value of EIS. As commented above,
541 our robust results with V_{sfc} suggest a linkage between cloud sensitivity to surface wind and
542 the poor representation of Sc clouds across a range of CMIP6 models.

543 Blanco et al. (2023; 2024) found that despite vertical velocity exerting the strongest
544 control on clouds over extratropical regions, it cannot explain the observed hemispheric

asymmetry of cloud albedo $\bar{C}$, which was attributed to a combination of V_{sfc}, SSTs, and the unique microphysical properties of Southern Ocean clouds. By similar arguments, it may be said that although EIS has been found to be the CCF that is best correlated with Sc clouds in the subsidence-dominated tropics, it may not be the largest contributor to the negative $\bar{C}$ biases. Further work could seek to explore whether inversion strength is more reasonably represented by models within the Australian region compared to the other four areas, and if so, whether it is in fact allowing for a better representation of cloud albedo sensitivity to surface wind in that region.

6. Summary and Conclusions

Marine stratocumulus clouds prevail in regimes of large-scale subsidence and strong inversions over tropical and subtropical regions, but they are underrepresented by successive generations of CMIP models and are the cornerstone of the large tropical cloud feedback uncertainties for a warming planet.

In this study we evaluated cloud albedo and its controlling factors from 15 CMIP6 models in atmosphere-only and coupled configurations against satellite observations and reanalysis. By the application of a simple framework to a reduced set of large-scale variables over five typical oceanic Sc areas, we found that:

-- Large ensemble-mean climatological cloud albedo biases occur in three of the areas: these are the Peruvian, Namibian and Californian regions. Over all five regions model spread is substantial.

-- Reduced annual-mean biases for a given model may result from compensation errors, especially over the Canarian and Australian regions. The former tends to produce excessive albedo associated with weak winds, whereas the latter overpredicts albedo in ascending regimes.

-- CMIP6 underrepresentation of inversion strength can partly explain the negative $\bar{C}$ biases, although other factors should also be responsible (as inferred from Črnivec et al. 2023 and our eqns. 1–2).

-- The negative $\bar{C}$ biases are linked to very poor, unrealistic cloud albedo sensitivity to surface wind in all models: against all theoretical and empirical evidence, simulated cloud albedo either varies little or decreases with increasing V_{sfc}.

In agreement with past studies spanning successive CMIP generations, our results indicate that underlying physical processes of cloud formation, maintenance and/or suppression occurring over marine tropical regions are necessarily missing or poorly represented, revealing parameterization problems in boundary layer and/or microphysical schemes. This arises not only from the aforementioned deficiency in models to simulate enhanced cloudiness under strengthening winds, but also from the lack of skill of many of them to simulate less cloudiness (at times substantially more) under sea surface warming in the coupled configuration compared to the atmosphere-only simulations, as would be the case from low-cloud –SST feedback expectations.

One possible application of our results is that the $C_{V_{sfc}}$ functions for models and observations may potentially act as a proxy for parameterization errors. The study of B24 showed for the same set of CMIP6 models that C_{SST} functions could analogously be used to detect common Southern Ocean cloud albedo biases associated with little/no supercooled liquid water (more reflective than glaciated cloud particles). This proposal of a diagnostic tool to evaluate $\bar{C}$ biases in tropical marine Sc regions is not the first of this type (e.g. Mochizuki et al 2007). Nevertheless, our method is advantageous for additional reasons: no sub-daily data or specific parameterization variables are required, and it allows for a straightforward intercomparison across a range of models.

Improving the representation of stratocumulus cloud is a major challenge to the modeling community due their unique complexity, with a delicate interplay between dynamics, microphysics and radiation. Lee et al (2022) found that increased vertical and horizontal resolution is beneficial for marine stratocumulus representation over coastal regions, although such improvements were not necessarily found further west in the oceanic basins. In another example, Peng et al (2024) found with a high-resolution multi-scale model that enhanced hyperviscosity (i.e. smoothing out wind) increases Sc amounts over the subtropical oceans, via a reduction of entrainment. Targeting simultaneously parameterization issues and coarse resolution problems, Nowak et al (2025) recently presented a 4-year global climatology of low-level clouds obtained from a storm resolving model (km-scale) with promising results.

Finally, our results have implications for changing climates. Observational studies have identified global and regional trends towards stronger surface winds over oceans in the twentieth century (Young et al., 2011; Servain et al., 2014) whereas climate simulations

predict changes in ocean wind speeds for the near future (McInnes et al., 2011; Hemer et al., 2013). Given the current status of Sc representation in the tropics, biases (and uncertainty) should amplify were tropical surface winds to strengthen, as inferred from a straightforward application of our CCF method to predict changes in $\bar{C}$. Assuming 1) time-invariant $C_{V_{sfc}}$ for both actual climate and models; 2) cloud albedo is function of surface wind *only* (one-dimensionality); and 3) a perfect prediction of future winds (i.e.: $P^{M}_{V_{sfc}} = P^{actual}_{V_{sfc}}$), then the shifting of $P_{V_{sfc}}$ distributions to stronger winds implies (via eq. 1) a much smaller increase (or even decrease) in Sc clouds as seen by models compared to the large $\bar{C}$ increase that would occur in reality. This simple, idealized exercise highlights the importance of using observational-constraining techniques that circumvent the problems of cloud parameterizations (in essence multidimensional combinations of P^{M}_{x} and C^{OBS}_{x} to estimate future $\bar{C}$) in the assessment of low-cloud feedback under global warming.

Acknowledgements

JEB is grateful to Casey Wall, Sam Dahl, Lisa Alexander and Steven Siems for their helpful comments to improve this manuscript.

Contributions

JEB was responsible for the study conception, design, and analysis, and drafted the first version of the manuscript. RC critically revised the manuscript to improve it to its current version, including discussion of the data, methodology, presentation of results, and discussion and conclusions sections. Both authors have read and approved the final manuscript.

Funding

This study was partially supported by the European Union's Horizon 2020 research and innovation program (CONSTRAIN, Grant 820829).

Ethics declarations

The authors declare no competing interests.

Data availability Statement

All data used here are available from CERES, ERA5 and CMIP6 online archives:

https://ceres-tool.larc.nasa.gov/ord-tool/jsp/SYN1degEd41Selection.jsp

https://www.ecmwf.int/en/forecasts/datasets/reanalysis-datasets/era5

https://pcmdi.llnl.gov/CMIP6/Guide/dataUsers.html

References

Aerenson, T., and Marchand, R., 2025: How do differences in the simulation of present-day clouds affect cloud feedbacks? J. Geophys. Res. Atmos., 130, e2025JD044020. DOI:10.1029/2025JD044020.

Bellomo, K., Clement, A., Mauritsen, T., Rädel, G., and Stevens, B., 2014: Simulating the Role of Subtropical Stratocumulus Clouds in Driving Pacific Climate Variability, J. Clim., 27, 5119–5131. DOI:10.1175/JCLI-D-13-00548.1.

Bellomo, K., Clement, A. C., Mauritsen, T., Rädel, G.,and Stevens, B., 2015: The Influence of Cloud Feedbacks on Equatorial Atlantic Variability, J. Clim., 28, 2725–2744. DOI:10.1175/JCLI-D-14-00495.1.

Bender, F. A., A. Engström, and J. Karlsson, 2016: Factors Controlling Cloud Albedo in Marine Subtropical Stratocumulus Regions in Climate Models and Satellite Observations. J. Clim., 29, 3559–3587, DOI:10.1175/JCLI-D-15-0095.1.

Bender, F. A. M., Frey, L., McCoy, D. T., Grosvenor, D. P., and Mohrmann, J. K., 2019: Assessment of aerosol–cloud–radiation correlations in satellite observations, climate models and reanalysis, Clim. Dynam., 52, 4371–4392, DOI:10.1007/s00382-018-4384-z.

Blanco, J. E., R. Caballero, G. Datseris, B. Stevens, S. Bony, O. Hadas, and Y. Kaspi, 2023: A Cloud-Controlling Factor Perspective on the Hemispheric Asymmetry of Extratropical Cloud Albedo. J. Clim., 36, 1793–1804. DOI:10.1175/JCLI-D-22-0410.1.

Blanco, J. E., R. Caballero, S. Sherwood, and L. Alexander, 2024: Insights into Cloud Albedo Biases from a Cloud-Controlling Factor Framework. J. Clim., 38, 563–581, DOI:10.1175/JCLI-D-24-0260.1.

Bock, L. and Lauer, A., 2024: Cloud properties and their projected changes in CMIP models with low to high climate sensitivity, Atmos. Chem. Phys., 24, 1587–1605, DOI:10.5194/acp-24-1587-2024.

Bony, S., and J.-L. Dufresne, 2005: Marine boundary layer clouds at the heart of tropical cloud feedback uncertainties in climate models. Geophys. Res. Lett., 32, L20806, DOI:10.1029/2005GL023851.

Boucher, O., D. A. Randall, N. Artaxo, C. Bretherton, G. Feingold, P. Forster, V.-M. Kerminen, Y. Kondo, H. Liao, U. Lohmann, P. Rasch, S. K. Satheesh, S. Sherwood, B. Stevens, and X.-Y. Zhang, 2013: Clouds and aerosols. Climate Change 2013: The Physical Science Basis. Contribution of Working Group I to the Fifth Assessment Report of the Intergovernmental Panel on Climate Change. Cambridge University Press, Cambridge, UK and New York, USA, 571–657.

Bretherton, C. S., and P. N. Blossey, 2014: Low cloud reduction in a greenhouse-warmed climate: Results from Lagrangian LES of a subtropical marine cloudiness transition. J. Adv. Model. Earth Syst., 6, 91–114. DOI:10.1002/2013MS000250.

Bretherton, C. S., P. N. Blossey, and C. R. Jones, 2013: Mechanisms of marine low cloud sensitivity to idealized climate perturbations: A single-LES exploration extending the CGILS cases. J. Adv. Model. Earth Syst., 5, 316–337, doi:10.1002/jame.20019.

Breul, P., Ceppi, P., and Nowack, P., 2025: The importance of stratocumulus clouds for projected warming patterns and circulation changes. Atmos. Chem. Phys., 25, 11991–12005, DOI:10.5194/acp-25-11991-2025.

Brient F., Roehrig, R., and Voldoire, A., 2019: Evaluating marine stratocumulus clouds in the CNRM-CM6-1 model using short-term hindcasts. J. Adv. Model. Earth Syst., 11, 127–148. DOI:10.1029/2018MS001461.

Brown, P. T., Lozier, M. S., Zhang, R., and Li, W., 2016: The necessity of cloud feedback for a basin-scale Atlantic Multidecadal Oscillation, Geophys. Res. Lett., 43, 3955–3963. DOI:10.1002/2016GL068303.

Burgman, R. J., Kirtman, B. P., Clement, A. C., and Vazquez, H., 2017: Model evidence for low-level cloud feedback driving persistent changes in atmospheric circulation and regional hydroclimate, Geophys. Res. Lett., 44, 428–437. DOI:10.1002/2016GL071978.

Caldwell, P. M., Y. Zhang, and S. A. Klein, 2013: CMIP3 Subtropical Stratocumulus Cloud Feedback Interpreted through a Mixed-Layer Model. J. Clim., 26, 1607–1625, DOI:10.1175/JCLI-D-12-00188.1.

Caldwell, P., and C. S. Bretherton, 2009: Response of a Subtropical Stratocumulus-Capped Mixed Layer to Climate and Aerosol Changes. J. Clim., 22, 20–38. DOI:10.1175/2008JCLI1967.1.

Ceppi, P., Brient, F., Zelinka, M.D. and Hartmann, D.L., 2017: Cloud feedback mechanisms and their representation in global climate models. WIREs Clim Change, 8: e465. DOI:10.1002/wcc.465

Ceppi, P., Myers, T. A., Nowack, P., Wall, C. J., and Zelinka, M. D., 2024: Implications of a pervasive climate model bias for low-cloud feedback. Geophys. Res. Lett., 51, e2024GL110525. DOI:10.1029/2024GL110525.

Cesana, G., Del Genio, A. D., and Chepfer, H.: The Cumulus And Stratocumulus CloudSat-CALIPSO Dataset (CASCCAD), 2019. Earth Syst. Sci. Data, 11, 1745–1764, DOI:10.5194/essd-11-1745-2019.

Cesana, G. V., A. S. Ackerman, N. Črnivec, R. Pincus, and H. Chepfer, 2023: An observation-based method to assess tropical stratocumulus and shallow cumulus clouds and

feedbacks in CMIP6 and CMIP5 models. Environ. Res. Commun., 5, 045001, DOI:/10.1088/2515-7620/acc78a.

Cutler, L., Brunke, M. A., and Zeng, X, 2022: Re-evaluation of low cloud amount relationships with lower tropospheric stability and estimated inversion strength. Geophys. Res. Lett., 49, e2022GL098137. DOI:10.1029/2022GL098137.

Črnivec, N., Cesana, G., and Pincus, R., 2023: Evaluating the representation of tropical stratocumulus and shallow cumulus clouds as well as their radiative effects in CMIP6 models using satellite observations. J. Geophys. Res. Atmos., 128, e2022JD038437. DOI:10.1029/2022JD038437

Dal Gesso, S., Van der Dussen, J., Siebesma, A., De Roode, S., Boutle, I., Kamae, Y., Roehrig, R., and Vial, J., 2015: A single-column model intercomparison on the stratocumulus representation in present-day and future climate. J. Adv. Model. Earth Syst., 7, 617–647. DOI:10.1002/2014MS000377.

De Roode, S. R., A. P. Siebesma, S. Dal Gesso, H. J. J. Jonker, J. Schalkwijk, and J. Sival, 2014: A mixed-layer model study of the stratocumulus response to changes in large-scale conditions, J. Adv. Model. Earth Syst., 6, 1256–1270. DOI:10.1002/2014MS000347.

de Szoeke, S. P., S. Yuter, D. Mechem, C. W. Fairall, C. D. Burleyson, and P. Zuidema, 2012: Observations of stratocumulus clouds and their effect on the eastern Pacific surface heat budget along 20°S. J. Clim., 25, 8542–8567. DOI:10.1175/JCLI-D-11-00618.1.

Donohoe, A., and D. S. Battisti, 2011: Atmospheric and surface contributions to planetary albedo. J. Clim., 24(16), 4402–4418, DOI:10.1175/2011JCLI3946.1.

Duynkerke, P. G., and J. Teixeira, 2001: Comparison of the ECMWF reanalysis with FIRE I observations: Diurnal variation of marine stratocumulus. J. Clim., 14,1466–1478. DOI:10.1175/1520-0442(2001)014<1466:COTERW>2.0.CO;2.

Ekman, A.M.L., Nygren, E., Pérez, A.B., Schwarz, M., Svensson, G. and Bellouin, N., 2023: Influence of horizontal resolution and complexity of aerosol–cloud interactions on marine

stratocumulus and stratocumulus-to-cumulus transition in HadGEM3-GC3.1. Quart. J. Roy. Meteor. Soc., 149(755), 2049–2066. DOI:10.1002/qj.4494.

Eyring, V., Bony, S., Meehl, G. A., Senior, C. A., Stevens, B., Stouffer, R. J., and Taylor, K. E. 2016: Overview of the Coupled Model Intercomparison Project Phase 6 (CMIP6) experimental design and organization, Geosci. Model Dev., 9, 1937–1958, DOI:10.5194/gmd-9-1937-2016.

Fons, E., Naumann, A. K., Neubauer, D., Lang, T., and Lohmann, U. 2024: Investigating the sign of stratocumulus adjustments to aerosols in the ICON global storm-resolving model, Atmos. Chem. Phys., 24, 8653–8675. DOI:10.5194/acp-24-8653-2024.

Hartmann, D. L., M. E. Ockert-Bell, and M. L. Michelsen, 1992: The Effect of Cloud Type on Earth's Energy Balance: Global Analysis. J. Clim., 5, 1281–1304. DOI:10.1175/1520-0442(1992)005<1281:TEOCTO>2.0.CO;2.

Hemer, M. A., Fan, Y., Mori, N., Semedo, A., and Wang, X. L.: Projected changes in wave climate from a multi-model ensemble, Nat. Clim. Change, 3, 471–476. DOI:10.1038/nclimate1791, 2013.

Hersbach H. and coauthors, 2020: The ERA5 global reanalysis Quart. J. Roy. Meteor. Soc., 146 (730), 1999-2049. DOI:10.1002/qj.3803.

Hourdin, F., A. Găinusă-Bogdan, P. Braconnot, J.-L. Dufresne, A.-K. Traore, and C. Rio, 2015: Air moisture control on ocean surface temperature, hidden key to the warm bias enigma. Geophys. Res. Lett., 42, 10,885–10,893, DOI:10.1002/2015GL066764.

Hsiao, W.-T., Hwang, Y.-T., Chen, Y.-J., and Kang, S. M., 2022: The Role of Clouds in Shaping Tropical Pacific Response Pattern to Extratropical Thermal Forcing, Geophys. Res. Lett., 49, e2022GL098023. DOI:10.1029/2022GL098023.

Jian, B., Li, J., Wang, G., Zhao, Y., Li, Y., Wang, J., Zhang, M., and Huang, J. 2021: Evaluation of the CMIP6 marine subtropical stratocumulus cloud albedo and its controlling factors, Atmos. Chem. Phys., 21, 9809–9828. DOI:10.5194/acp-21-9809-2021.

803 Kawai H. and S. Shige, 2020: Marine Low Clouds and their Parameterization in Climate
804 Models, J. Meteorol. Soc. Japan. Ser. II, Vol 98, 6, 1097-1127, DOI:10.2151/jmsj.2020-059.

805

806 Karlsson, J., Svensson, G. and Rodhe, H., 2008: Cloud radiative forcing of subtropical low
807 level clouds in global models. Clim. Dyn. 30, 779–788. DOI:10.1007/s00382-007-0322-1.

808

809 Kazil, J., G. Feingold, and T. Yamaguchi, 2016: Wind speed response of marine non-
810 precipitating stratocumulus clouds over a diurnal cycle in cloud-system resolving
811 simulations. Atmos. Chem. Phys., 16, 5811–5839. DOI:10.5194/acp-16-5811-2016.

812

813 Kim, H., Kang, S. M., Kay, J. E., and Xie, S.-P., 2022: Subtropical clouds key to Southern
814 Ocean teleconnections to the tropical Pacific, P. Natl. Acad. Sci. USA, 119, e2200514119.
815 DOI:10.1073/pnas.2200514119.

816

817 Klein, S. A., and D. L. Hartmann, 1993: The seasonal cycle of low stratiform clouds. J.
818 Clim., 6, 1588–1606. DOI: 10.1175/1520-0442(1993)006<1587:TSCOLS>2.0.CO;2.

819

820 Klein, S.A., Hall, A., Norris, J.R. and Pincus R., 2017: Low-cloud feedbacks from cloud-
821 controlling factors: A review. Surv. Geophys. 38, 1307-1329. DOI:10.1007/s10712-017-
822 9433-3.

823

824 Klein, S.A., Y. Zhang, M.D. Zelinka, R. Pincus, J. Boyle, and P. J.Gleckler, 2013: Are
825 climate model simulations of clouds improving? An evaluation using the ISCCP simulator, J.
826 Geophys. Res. Atmos., 118, 1329–1342. DOI:10.1002/jgrd.50141.

827

828 Konsta, D., Dufresne, J.-L., Chepfer, H., Vial, J., Koshiro, T., Kawai, H., Bodas-Salcedo, A.,
829 Roehrig, R., Watanabe, M., and Ogura, T., 2022: Low-level marine tropical clouds in six
830 CMIP6 models are too few, too bright but also too compact and too homogeneous. Geophys.
831 Res. Lett., 49, e2021GL097593. DOI:10.1029/2021GL097593.

832

833 Koshiro, T., M. Shiotani, H. Kawai, and S. Yukimoto, 2018: Evaluation of relationships
834 between subtropical marine low stratiform cloudiness and estimated inversion strength in
835 CMIP5 models using the satellite simulator package COSP. SOLA, 14, 25–32.
836 DOI:10.2151/sola.2018-005.

837

838 Koshiro, T., H. Kawai, and A.T. Noda, 2022: Estimated cloud-top entrainment index explains
839 positive low-cloud-cover feedback. Proc. Natl. Acad. Sci. U.S.A. 119 (29) e2200635119,
840 DOI:10.1073/pnas.2200635119.

841

842 Lauer, A., and K. Hamilton, 2013: Simulating Clouds with Global Climate Models: A
843 Comparison of CMIP5 Results with CMIP3 and Satellite Data. J. Clim., 26, 3823–3845,
844 DOI:10.1175/JCLI-D-12-00451.1.

845

846 Lee, H.-H., Bogenschutz, P., and Yamaguchi, T., 2022: Resolving away stratocumulus biases
847 in modern global climate models. Geophys. Res. Lett., 49, e2022GL099422.
848 DOI:10.1029/2022GL099422.

849

850 Lewis, H., and Bellon, G., 2025: Contextualizing GCM biases in low-cloud coverage: The
851 role of large-scale conditions. Geophys. Res. Lett.,52, e2025GL116330.
852 DOI:10.1029/2025GL116330.

853

854 Li, J.-L. F., Xu, K.-M., Lee, W.-L., Jiang, J. H., Tsai, Y.-C., Yu, J.-Y., and coauthors, 2023:
855 Warm clouds biases in CMIP6 models linked to indirect effects of falling ice-radiation
856 interactions over the tropical and subtropical Pacific. Geophys. Res. Lett., 50,
857 e2023GL104990. DOI:10.1029/2023GL104990.

858

859 Li, Y., D. W. J. Thompson, G. L. Stephens, and S. Bony, 2014: A global survey of the
860 instantaneous linkages between cloud vertical structure and large-scale climate, J. Geophys.
861 Res. Atmos., 119, 3770–3792. DOI:10.1002/2013JD020669.

862

863 Lin, J.-L., Qian, T., and Shinoda, T., 2014: Stratocumulus clouds in Southeastern Pacific
864 Simulated by eight CMIP5–CFMIP global climate models. J. Clim., 27(8), 3000–3022.
865 DOI:10.1175/jcli-d-13-00376.1.

866

867 Loeb, N. G., and Coauthors, 2018: Clouds and the Earth's Radiant Energy System (CERES)
868 Energy Balanced and Filled (EBAF) Top-of-Atmosphere (TOA) Edition-4.0 Data Product. J.
869 Clim., 31, 895–918. DOI:10.1175/JCLI-D-17-0208.1.

870

871 Ma, C., C. R. Mechoso, A. W. Robertson, and A. Arakawa, 1996: Peruvian Stratus Clouds
872 and the Tropical Pacific Circulation: A Coupled Ocean-Atmosphere GCM Study. J. Climate,
873 9, 1635–1645. DOI:10.1175/1520-0442(1996)009<1635:PSCATT>2.0.CO;2.

874

875 McInnes, K. L., Erwin, T. A., and Bathols, J. M., 2011: Global climate model projected
876 changes in 10m wind speed and direction due to anthropogenic climate change, Atmos. Sci.
877 Lett., 12, 325–333. DOI:10.1002/asl.341.

878

879 Mechoso, C., Wood, R., Weller, R., Bretherton, C. S., Clarke, A., Coe, H., Fairall, C., Farrar,
880 J. T., Feingold, G., Garreaud, R., Grados, C., McWilliams, J., De Szoeke, S. P., Yuter, S. E.,
881 & Zuidema, P. (2014). Ocean–cloud–atmosphere–land interactions in the southeastern
882 pacific: The vocals program. Bull. Am. Meterol. Soc., 95(3), 357–375. DOI:10.1175/BAMS-
883 D-11-00246.1.

884

885 Medeiros, B., B. Stevens, I. M. Held, M. Zhao, D. L. Williamson, J. G. Olson, and C. S.
886 Bretherton, 2008: Aquaplanets, climate sensitivity, and low clouds. J. Clim., 21, 4974–4991,
887 doi:10.1175/2008JCLI1995.1.

888

889 Meehl, G. A., Boer, G. J., Covey, C., Latif, M., and Stouffer, R. J. 2000: The Coupled Model
890 Intercomparison Project (CMIP), Bull. Am. Meteorol. Soc., 81, 313–318.

891

892 Mellado, J. P., 2017: Cloud-top entrainment in stratocumulus clouds. Annual Review of Fluid
893 Mechanics, 49, 145–169. DOI:10.1146/annurev-fluid-010816-06023.1

894

895 Middlemas, E. A., Clement, A. C., Medeiros, B., and Kirtman, B., 2019: Cloud Radiative
896 Feedbacks and El Niño–Southern Oscillation, J. Clim., 32, 4661–4680, DOI:10.1175/JCLI-
897 D-18-0842.1.

898

899 Mieslinger, T., Á. Horváth, S. A. Buehler, and M. Sakradzija, 2019: The dependence of
900 shallow cumulus macrophysical properties on large-scale meteorology as observed in ASTER
901 imagery. J. Geophys. Res. Atmos., 124, 11 477–11 505. DOI:10.1029/2019JD030768.

902

903 Mochizuki, T., T. Miyama, and T. Awaji, 2007: A simple diagnostic calculation of marine
904 stratocumulus cloud cover for use in general circulation models, J. Geophys. Res., 112,
905 D06113. DOI:10.1029/2006JD007223.

Muhlbauer, A., McCoy, I. L., and Wood, R., 2014: Climatology of stratocumulus cloud morphologies: microphysical properties and radiative effects. Atmos. Chem. Phys., 14, 6695–6716. DOI:10.5194/acp-14-6695-2014.

Myers, T. A., and Norris, J. R., 2013: Observational evidence that enhanced subsidence reduces subtropical marine boundary layer cloudiness. J. Clim., 26(19), 7507–7524. DOI:10.1175/JCLI-D-12-00736.1.

Myers, T. A., and J. R. Norris, 2015: On the relationships between subtropical clouds and meteorology in observations and CMIP3 and CMIP5 models. J. Clim., 8, 2945–2967, DOI:10.1175/JCLI-D-14-00475.1.

Myers, T. A., R. C. Scott, M. D. Zelinka, S. A. Klein, J. R. Norris, and P. M. Caldwell, 2021: Observational constraints on low cloud feedback reduce uncertainty of climate sensitivity. Nat. Climate Change, 11, 501–507. DOI:10.1038/s41558-021-01039-0.

Myers, T.A., Vogel, R., Brient, F., Parishani, H. and Scott, R.C., 2023: Tropical Marine Low Clouds: Feedbacks to Warming and on Climate Variability. In Clouds and Their Climatic Impacts (eds S.C. Sullivan and C. Hoose). DOI:10.1002/9781119700357.ch7.

Nam, C., S. Bony, J.-L. Dufresne, and H. Chepfer, 2012: The 'too few, too bright' tropical low-cloud problem in CMIP5 models, Geophys. Res. Lett., 39, L21801. DOI:10.1029/2012GL053421.

Noda, A. T., Nakamura, K., Iwasaki, T., & Satoh, M. (2014). Responses of subtropical marine stratocumulus cloud to perturbed lower atmospheres. SOLA, 10, 34–38. DOI:10.2151/sola.2014-008.

Nowak, J. L., Dragaud, I. C. D. V., Lee, J., Dziekan, P., Mellado, J. P., and Stevens, B., 2025: A first look at the global climatology of low-level clouds in storm resolving models. J. Adv. Model. Earth Syst., 17, e2024MS004340. DOI:10.1029/2024MS004340.

939 Nuijens, L. and Siebesma, A.P., 2019: Boundary Layer Clouds and Convection over
940 Subtropical Oceans in our Current and in a Warmer Climate. Curr. Clim. Change Rep. 5, 80–
941 94. DOI:10.1007/s40641-019-00126-x.

942

943 Nuijens, L., and B. Stevens, 2012: The influence of wind speed on shallow marine cumulus
944 convection. J. Atmos. Sci., 69, 168–184. DOI:10.1175/JAS-D-11-02.1.

945

946 Peng, L., Blossey, P. N., Hannah, W. M., Bretherton, C. S., Terai, C. R., Jenney, A. M., and
947 Pritchard, M., 2024: Improving stratocumulus cloud amounts in a 200-m resolution multi-
948 scale modeling framework through tuning of its interior physics. J. Adv. Model. Earth Syst.,
949 16, e2023MS003632. DOI:10.1029/2023MS003632

950

951 Qu, X., A. Hall, S. A. Klein, and P. M. Caldwell, 2014: On the spread of changes in marine
952 low cloud cover in climate model simulations of the 21st century. Climate Dyn., 42, 2603–
953 2626. DOI:10.1007/s00382-013-1945-z.

954

955 Qu X., Hall A., Klein S.A., DeAngelis A.M., 2015: Positive tropical marine low-cloud cover
956 feedback inferred from cloud-controlling factors. Geophys. Res. Lett. 42:7767–7775.
957 DOI:10.1002/2015GL065627

958

959 Rieck, M., L. Nuijens, and B. Stevens, 2012: Marine boundary layer cloud feedbacks in a
960 constant relative humidity atmosphere. J. Atmos. Sci., 69, 2538–2550, DOI:10.1175/JAS-D-
961 11-0203.1.

962

963 Salazar, A. M., B. Medeiros, J. Zhu, and E. Tziperman, 2025: Investigating the Effects of a
964 Subtropical Stratocumulus Cloud Breakup in Warm Climates Using Cloud-Locking
965 Experiments. J. Clim., 38, 4315–4330. DOI:10.1175/JCLI-D-24-0371.1.

966

967 Schneider, T., C. M. Kaul, and K. G. Pressel, 2019: Possible climate transitions from breakup
968 of stratocumulus decks under greenhouse warming. Nat. Geosci., 12, 163–167.
969 DOI:10.1038/s41561-019-0310-1.

970

971 Scott, R. C., T. A. Myers, J. R. Norris, M. D. Zelinka, S. A. Klein, M. Sun, and D. R.
972 Doelling, 2020: Observed Sensitivity of Low-Cloud Radiative Effects to Meteorological

973 Perturbations over the Global Oceans. J. Clim., 33, 7717–7734. DOI:10.1175/JCLI-D-19-
974 1028.1.

975

976 Seethala, C., J. R. Norris, and T. A. Myers, 2015: How Has Subtropical Stratocumulus and
977 Associated Meteorology Changed since the 1980s? J. Clim., 28, 8396–8410,
978 DOI:10.1175/JCLI-D-15-0120.1.

979

980 Servain, J., Caniaux, G., Kouadio, Y. K., McPhaden, M. J., and Araujo, M., 2014: Recent
981 climatic trends in the tropical Atlantic, Clim. Dynam., 43, 3071–3089, doi:10.1007/s00382-
982 014-2168-7.

983

984 Siebesma, A. P., C. Jakob, G. Lenderink, R. A. J. Neggers, J. Teixera, E. Van Meijgaard, J.
985 Calvo, A. Chlond, H. Grenier, C. Jones, M. Köhler, H. Kitagawa, P. Marquet, A. P. Lock, F.
986 Müller, D. Olmeda, and C. Serverijns, 2004: Cloud representation in general circulation
987 models over the northern Pacific Ocean: A EUROCS intercomparison study. Quart. J. Roy.
988 Meteor. Soc., 130, 3245–3267. DOI:10.1256/qj.03.146.

989

990 Stephens, G.L., D. O'Brien, P.J. Webster, P. Pilewski, S. Kato and J.-l. Li, 2015: The albedo
991 of Earth, Rev. Geophys., 53, 141–163.

992

993 Stevens, B., 2005: Atmospheric moist convection. Annu. Rev. Earth Planet. Sci., 33, 605–
994 643. DOI:10.1146/annurev.earth.33.092203.122658.

995

996 Stevens, B., 2024: A perspective on the future of CMIP. AGU Advances, 5,
997 e2023AV001086. DOI:10.1029/2023AV001086.

998

999 Su, H., J. H. Jiang, C. Zhai, V. S. Perun, J. T. Shen, A. D. Del Genio, L. S. Nazarenko, L. J.
1000 Donner, L. W. Horowitz, C. J. Seman, C. J. Morcrette, J. Petch, M. A. Ringer, J. Cole, M. d.
1001 S. Mesquita, T. Iversen, J. E. Kristjansson, A. Gettelman, L. D. Rotstayn, S. J. Jeffrey, J.-L.
1002 Dufresne, M. Watanabe, H. Kawai, T. Koshiro, T. Wu, E. M. Volodin, T. L'Ecuyer, J.
1003 Teixeira, and G. L. Stephens, 2013: Diagnosis of regime-dependent cloud simulation errors in
1004 CMIP5 models using "A-Train" satellite observations and reanalysis data. J. Geophys. Res.:
1005 Atmos., 118, 2762–2780. DOI:10.1029/2012JD018575.

1006

van der Dussen, J. J., de Roode, S. R., and Siebesma, A. P., 2014: Factors controlling rapid stratocumulus cloud thinning. J. Atmos. Sci., 71(2), 655–664. DOI:10.1175/JAS-D-13-0114.1.

van der Dussen, J. J., de Roode, S. R., and Siebesma, A. P., 2016: How large-scale subsidence affects stratocumulus transitions. Atmos. Chem. Phys., 16(2), 691–701. DOI:10.5194/acpd-15-17229-2015.

Voigt, A., Shaw, T., 2015: Circulation response to warming shaped by radiative changes of clouds and water vapour. Nature Geosci 8, 102–106. DOI:10.1038/ngeo2345.

Rädel, G., Mauritsen, T., Stevens, B., Dommenget, D., Matei, D., Bellomo, K., and Clement, A., 2016: Amplification of El Niño by cloud longwave coupling to atmospheric circulation, Nat. Geosci., 9,106–110 DOI:10.1038/ngeo2630.

Voigt A., Albern N., Ceppi P., Grise K., Li Y., Medeiros B., 2021: Clouds, radiation, and atmospheric circulation in the present-day climate and under climate change. WIREs Clim Change, 12: e694. DOI:10.1002/wcc.694.

Wang, H., Rasch, P. J., and Feingold, G., 2011: Manipulating marine stratocumulus cloud amount and albedo: a process-modelling study of aerosol-cloud-precipitation interactions in response to injection of cloud condensation nuclei, Atmos. Chem. Phys., 11, 4237–4249, DOI:10.5194/acp-11-4237-2011.

Weare, B., 2004: A comparison of AMIP II model cloud layer properties with ISCCP D2 estimates, Clim. Dyn., 22, 281–292. DOI:10.1007/s00382-003-0374-9.

Webb, M., C. Senior, S. Bony, and J.-J. Morcrette, 2001: Combining ERBE and ISCCP data to assess clouds in the Hadley Centre, ECMWF and LMD atmospheric climate models, Clim. Dyn., 17(12), 905–922. DOI:10.1007/s003820100157.

Williams, K. D. and Bodas-Salcedo, 2017: A.: A multi-diagnostic approach to cloud evaluation, Geosci. Model Dev., 10, 2547–2566. DOI:10.5194/gmd-10-2547-2017.

Wood, R., 2012: Stratocumulus Clouds. Mon. Wea. Rev., 140, 2373–2423, DOI:10.1175/MWR-D-11-00121.1.

Wood, R., and C. S. Bretherton, 2006: On the Relationship between Stratiform Low Cloud Cover and Lower-Tropospheric Stability. J. Clim., 19, 6425–6432, DOI:10.1175/JCLI3988.1.

Young, I. R., Zieger, S., and Babanin, A. V., 2011: Global trends in wind speed and wave height, Science, 332, 451–455. DOI:10.1126/science.1197219.

Zhang, M., Lin, W., Klein, S., Bacmeister, J., Bony, S., Cederwall, R., Del Genio, A., Hack, J., Loeb, N., Lohmann, U., Minnis, P., Musat, I., Pincus, R., Stier, P., Suarez, M. J., Webb, M. J., Wu, J. B., Xie, S. C., Yao, M.-S., and Zhang, J. H., 2005: Comparing clouds and their seasonal variations in 10 atmospheric general circulation models with satellite measurements, J. Geophys. Res. Atmos., 110, D15S02. DOI:10.1029/2004JD005021.

Zhang, J. and Feingold, G., 2023: Distinct regional meteorological influences on low-cloud albedo susceptibility over global marine stratocumulus regions, Atmos. Chem. Phys., 23, 1073–1090. DOI:10.5194/acp-23-1073-2023.

Zhang, Q., Liu, B., Li, S., and Zhou, T., 2023: Understanding models' global sea surface temperature bias in mean state: From CMIP5 to CMIP6. Geophys. Res. Lett., 50, e2022GL100888. DOI:10.1029/2022GL100888.

Supplementary Files

This is a list of supplementary files associated with this preprint. Click to download.

- SUPPL33.docx